RSC Advances

PAPER

View Article Online
View Journal | View Issue

Cite this: *RSC Adv.*, 2017, **7**, 25848

Gold coated iron phosphide core–shell structures†

Anna T. Kelly,[a] Carly S. Filgueira,[a] Desmond E. Schipper,[a] Naomi J. Halas[ab] and Kenton H. Whitmire*[a]

Received 26th January 2017
Accepted 8th May 2017

DOI: 10.1039/c7ra01195d

rsc.li/rsc-advances

Core–shell particles Fe_2P@Au have been prepared beginning with Fe_2P nanorods, nanocrosses and nanobundles prepared from the solvothermal decomposition of $H_2Fe_3(CO)_9(\mu_3\text{-}P^tBu)$. Iron phosphide structures can be produced from a single-source organometallic precursor with morphological control by varying the surfactant conditions to yield fiber bundles and dumbbell-shaped bundles ranging from nanometers to microns. Derivatization of the surfaces with γ-aminobutyric acid was used to attach Au nanoparticle seeds to the surface of the Fe_2P nanoparticles followed by completion of the Au shell by reduction with formaldehyde or aqueous $HAuCl_4$/CO, with the latter giving somewhat better results. Shell thickness ranged from an incomplete, partially coated Au shell to a thickness of 65 ± 21 nm by varying the amount of gold decorated precursor particles. Increasing the thicknesses of the Au shells produced a redshift in the plasmonic resonance of the resulting structures as was observed previously for FeO_x@Au.

Introduction

Much insight has been gained into the control of the size and shape of nanoparticles over the past few years, which in turn allows for their rational design by tuning their various properties. For example, magnetic nanoparticles have been investigated for use in catalysis, data storage, and biomedical applications.[1–6] Focus has now turned to combining nanoparticles having different properties to make multifunctional materials.[7] Some studies have examined the coupling of catalysts with magnetic nanoparticles for easy recovery of the catalyst.[8,9] Other systems have combined magnetic nanoparticles with fluorescent semiconductor quantum dots to obtain multifunctional nanoparticle systems.[10]

When incorporating magnetic nanoparticles into systems intended for biological applications, careful consideration must be taken to ensure the biocompatibility of the system. Magnetic nanoparticles are often synthesized in organic media and capped with long chain organic surfactants. Therefore, surface functionalization of these particles must be performed to make them biocompatible, one example being the use of starch-coated superparamagnetic iron oxide nanoparticles for *in vitro* thermal ablation of cancer cells.[11] A variety of successful approaches for the functionalization and incorporation of magnetic nanoparticles into biological systems have been reported.[12–14]

The combination of gold with magnetic nanoparticles in a core–shell structure presents an interesting bifunctional system. Gold is well-known for its biocompatibility and plasmonic properties, making it an optimal choice for the surface-coating of a variety of nanoparticles to produce a non-toxic, water soluble material that can be optically tracked within the body. The gold surface, being relatively chemically inert, resists oxidation and provides protection for the core particle. Additionally, owing to its high electron density, gold can be visualized easily by microscopy.

Gold has been used to coat diamond, metal, metal alloy and metal oxide nanoparticles for uses in plasmonic materials, catalysis and medical diagnostics and treatment.[15–26] We have reported the use of faceted or tetracubic iron oxide nanoparticles as cores coated with a gold shell layer.[27] In this work, it was shown that substitution of the core with a nonspherical morphology results in differences in the optical properties of these materials due to the reduction of symmetry introduced by variations in core geometry. When the spherical symmetry of the core was broken, new plasmon modes and larger shifts appeared in the spectrum, due to the mixing of plasmons of different multipolar symmetry. Other anisotropic core–Au shell morphologies have also been reported, including rice-shaped Fe_2O_3–Au[28] and Au–FeOOH nanomaterials.[29] Elongated structures are particularly interesting because they exhibit two plasmon resonances, transverse and longitudinal. The longitudinal plasmon is polarization dependent and its position is highly sensitive to the aspect ratio of the particles.[30,31]

We have been exploring the preparation of metal pnictide nanoparticles and thin films from single source precursors,

[a]*Department of Chemistry, MS60, Rice University, 6100 Main Street, Houston, TX 77005, USA. E-mail: whitmir@rice.edu*

[b]*Department of Electrical and Computer Engineering, MS366, Department of Physics and Astronomy, MS61, Rice University, 6100 Main Street, Houston, TX 77005, USA*

† Electronic supplementary information (ESI) available: Additional SEM and TEM images, summary of solution extinction data for core–shell structures made by CO reduction. Elemental maps from SEM/EDAX spectra of the gold-coated particles. See DOI: 10.1039/c7ra01195d

which has proven a successful method for preparing phase-pure materials. Using $H_2Fe_3(CO)_9(\mu_3\text{-}P^tBu)$ we have been able to prepare a variety of Fe_2P nanostructures including split bundles, T-shapes, and crosses.[32] These structures are prone to crystal splitting and a variety of morphologies can result, and they have magnetic moment values ranging from 2 to 3 μ_B at the saturation magnetization. We have also reported on the derivatization and coating of iron oxide nanoparticles with a gold shell along with their photonic properties.[27] Coupling magnetic and plasmonic properties in one particle increases functionality and attaining a continuous Au layer enhances solubility and promotes biocompatibility. For example, analytical techniques that rely on plasmonic properties, such as surface plasmon resonance and surface enhanced Raman spectroscopy can be combined with magnetic techniques, such as separation, isolation, and purification. The anisotropic morphology of Fe_2P structures is optically interesting because coupling between the plasmons will differ depending on the number and orthogonality of the particle arms. Two separate reducing agents were investigated for the reduction of gold onto the Fe_2P particle surface, formaldehyde and carbon monoxide. Both of these approaches are presented, along with the corresponding experimentally observed solution extinction spectra for varying degrees of shell thickness.

Experimental

General procedures

The Fe_2P nanorods and nanobundles were prepared as reported previously.[27,32] Gold(III) chloride hydrate, γ-aminobutanoic acid (GABA), and tetrakis(hydroxymethyl)-phosphonium chloride (THPC, 80% solution in water), were obtained from Aldrich. Formaldehyde (37% solution in water/ethanol) and potassium carbonate were purchased from Fisher Scientific. Carbon monoxide was obtained from Matheson TriGas. Milli-Q water was obtained from a Millipore Total Q system. Ultraviolet-Visible (UV-Vis) absorption studies were performed in aqueous solution in 1 cm path length polystyrene cuvettes (Fisher Scientific) on a Varian Cary 5000 UV-Vis-NIR scanning Spectrophotometer (300–1000 nm with 1 nm steps).

Core–shell nanostructure formation

The iron phosphide nanoparticles were coated with gold using a procedure based on that described by Oldenburg *et al.* for coating silica NPs.[33] The method was modified because the 3-aminopropyltrimethoxysilane (APTMS) used by Oldenburg *et al.* was not applicable to the iron phosphide system, as the $-Si(OMe)_3$ end of the molecule would not bind to the iron phosphide nanoparticles due to the absence of any oxygen atoms at the surface. Therefore, γ-aminobutanoic acid (GABA) was used instead, with the carboxylic acid functionality for binding to the surface of the Fe_2P nanoparticles and the amine group for the attachment of small (~1 to 2 nm) colloidal gold nanoparticles (Scheme 1). This ligand exchange step also served to increase the particles' water-dispersibility by replacing the hydrophobic oleic acid surfactant. The gold colloid (THPC gold

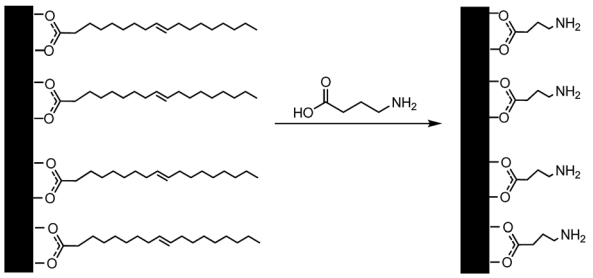

Scheme 1 Functionalization of the Fe_2P nanostructures with GABA *via* ligand exchange.

solution composed of 1–2 nm Au colloid) was prepared according to Duff *et al.*[34] Under rapid stirring, 1.2 mL of 1 M NaOH was added to 180 mL of H_2O, followed by the addition of 4 mL of a 1.2 mM aqueous THPC solution to yield a final THPC concentration of 2.6 μM. After 5 min of continuous stirring, 6.75 mL of 1 wt% aqueous chloroauric acid was added in one quick motion, after which the solution immediately turned to a medium brown color. The final solution was refrigerated and aged for at least 2 weeks before use. The product has a shelf life of ~6 months when stored at 4 °C.

In a typical procedure, 0.25 g of $H_2Fe_3(CO)_9(\mu_3\text{-}P^tBu)$ was placed in a mixture of tri-*n*-octylamine and oleic acid in a suitable ratio (*vide infra*) totalling approximately 8 mL. The solution was heated slowly to >320 °C, upon which the solution turned black indicating the formation of a colloidal solution. The solution was cooled and the particles were precipitated by addition of ~10 mL of ethanol. The supernatant was removed, and hexanes added to the flask. The resulting suspension was then transferred to a centrifuge tube; the resulting black solid was washed several times with hexanes to remove any residual surfactant. A solution of 0.10 g (1 mmol) of GABA dissolved in ~1–3 mL of deionized water was prepared in a scintillation vial. The iron phosphide particles were suspended in hexane (~5 mL) and added dropwise to this solution with vigorous stirring. The resulting solution was stirred overnight at room temperature. When the stirring was terminated, the less dense hexane layer was clear and the aqueous layer was dark gray, indicating that the surfactant exchange had been successful, producing water-dispersed iron phosphide particles. The particles could be isolated by centrifugation of the aqueous layer. A series of washes with water, involving the centrifugation of the sample followed by the removal of the supernatant and re-dispersion of the particles in water, were performed to remove any excess GABA present.

Decorated precursor nanoparticles were prepared by combining 40 mL of the colloidal gold solution with a concentrated solution of the GABA-functionalized iron phosphide nanoparticles in ethanol (~1 mL) and 4 mL of 1 M NaCl in a 50 mL centrifuge tube. The tube was shaken, then sonicated briefly and placed in a refrigerator overnight. The solution was centrifuged, leaving a small pellet at the bottom or side of the tube. The optimum centrifuge conditions were found to be 3000 rcf for 20–30 minutes. The supernatant was removed, and the precipitated solid was washed three times with deionized H_2O

by centrifugation at 3000 rcf for 30 min per centrifugation cycle to remove any excess free unbound colloidal gold (bright red color). When redispersed, the resulting pellet generated an aqueous suspension of gold-decorated nanoparticles purple in color.

Varying amounts of a stock solution of the Au-decorated precursor nanoparticles (*vide supra*) suspended in 5 mL DI H_2O were added to an aqueous potassium carbonate–gold(III) chloride hydrate (K_2CO_3/$HAuCl_4$) solution. The plating solution was made using 400 mL Milli-Q H_2O, 0.1 g K_2CO_3 (0.72 mmol), and 6 mL of an aqueous 1% $HAuCl_4$ solution (~0.02 mmol). These conditions were tested based on previous experiments with other core particles.[39] The colloidal gold on the surface of the Fe_2P nanostructures functioned as nucleation sites for the reduction of Au^{3+} to Au^0 using either formaldehyde or carbon monoxide. In the case of formaldehyde, 20 mL of formaldehyde solution was added to the decorated precursor/plating solution (50, 75, 100, or 125 μL of decorated precursor solution combined with 3 mL of plating solution) and the vial was shaken in order to initialize the reaction and ensure that the reduction was homogeneous throughout the solution. After extinction spectra were acquired, the solutions were centrifuged and washed with Milli-Q H_2O in order to stop the reaction and remove any residual formaldehyde. A similar procedure was followed employing CO reduction of the chloroauric acid. When CO was used as the reducing agent, 6 mL of the plating solution was combined with varying amounts of decorated precursor solution (25, 50, 75, 100, and 125 μL) in a vial and the solution was bubbled with CO for ~1 minute. As the solution was bubbled, the color changed to varying shades of pale gray to pink, depending on the thickness of the gold shell formed. The products were characterized using UV-Vis spectroscopy and TEM. TEM grids were prepared by dispersing the product nanoparticles in hexane (~5 mL) and drop casting onto the TEM (carbon-coated copper) grids. The solvent was evaporated and the sample analysed using JEOL 2000FX and JEOL 2010 microscopes.

Results and discussion

The rod, bundled-rod and crossed-bundle configurations of the Fe_2P particles led us to consider creating photonic materials based on their anisotropic shapes. Attempts to coat the Fe_2P nanoparticles directly with gold without prior functionalization, however, were not successful. The first step toward the formation of Fe_2P–Au core–shell structures was the functionalization of the Fe_2P nanoparticles to promote water solubility and introduce a linker for the attachment of small gold colloid. There are a variety of publications in which ligand exchange was used to transfer nanoparticles from organic to aqueous solutions.[35–39] In the case of silica–Au nanoshells, aminopropyltriethoxysilane (APTES) was used to functionalize the silica cores before the deposition of gold.[33] Previous reports for the synthesis of iron oxide nanoparticles with a gold shell used a ligand exchange reaction with an aminosilane (such as APTES) to displace the long-chain surfactants, resulting in hydrophilic nanoparticles.[28,40,41] This approach was attempted in the iron phosphide system, but was unsuccessful, likely because the functionalization with APTMS is thought to occur through the free hydroxide terminal groups on the surface of the nanoparticles that would bind easily to the silane moiety. As this kind of functionality is not present on the Fe_2P nanoparticles, a different approach was taken to the solubilization. Decoration of the core nanoparticles with colloidal gold is known to take place *via* the dative bonding of the lone pair of terminal $-NH_2$ groups to the gold nanoparticles,[41,42] as was seen in the functionalization of the aminosilane-coated iron oxide nanoparticles. The capping agent chosen was γ-aminobutyric acid (GABA) because it is a short-chain molecule with both amine and carboxylic acid functionalities. It was believed that the carboxylic acid would bind to the surface of the iron phosphide particles, displacing the oleic acid present in the original system, leaving the amine functionality available for binding to the colloidal gold nanoparticles. Fig. 1 shows an example of the Au-decorated Fe_2P nanorods.

Once the Au-decorated precursor nanoparticles were obtained, electroless gold plating was accomplished using an aqueous solution of $HAuCl_4$, which was reduced onto the nanoparticles using formaldehyde or carbon monoxide, forming a layer of gold around the Fe_2P nanoparticles similar to the methods used for preparation of APTMS-based materials.[40] The thickness of the gold shell is related to the amount of precursor solution added and the concentration of Au^{3+} in the solution. The general procedure for the formation of Au-coated Fe_2P nanoparticles is depicted in Scheme 2.

Formaldehyde has traditionally been used as the reducing agent in the synthesis of silica–Au nanoshells. However, Brinson *et al.* reported the use of carbon monoxide gas as the reducing agent to produce high quality, thin gold shell layers.[40] The results of both the formaldehyde and carbon monoxide reductions will be presented.

Formaldehyde reduction

Bundle-like particles synthesized from $H_2Fe_3(CO)_9P^tBu$ in a 1 : 1 system of TOA : OA were used for the experiments using

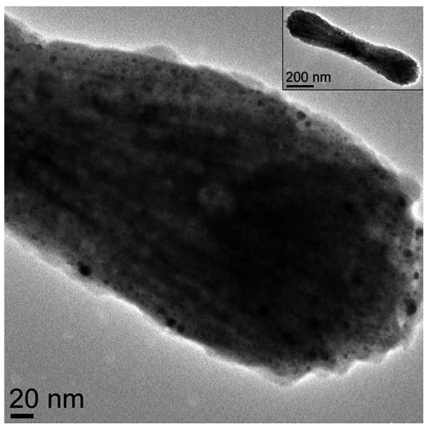

Fig. 1 TEM image of the Fe_2P nanorod after decoration with Au colloid (inset shows the entire nanorod).

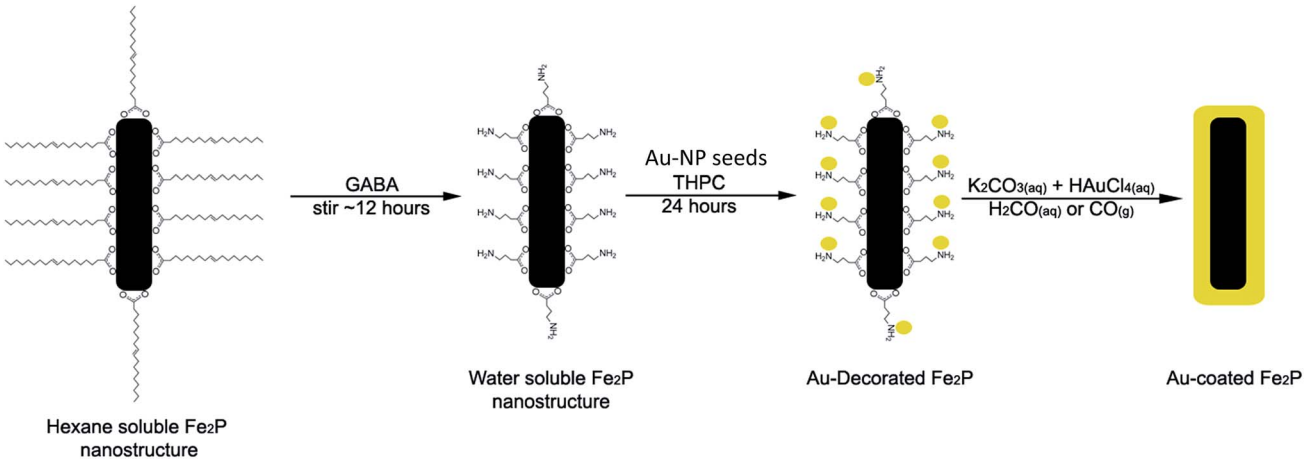

Scheme 2 General procedure for the coating of Fe_2P nanoparticles with gold to form Fe_2P–Au nanostructures (not to scale).

formaldehyde as the reducing agent. However, the same protocol is applicable for smaller fibers in the nano-range synthesized with other solvent ratios.[32] As described by Kelly *et al.*,[32] a lower solvent aspect ratio yields larger, bundle-like (split) structures and higher aspect ratio smaller, more rod-like structures. Fig. 2 depicts the nanoparticles before and after the treatment with GABA and decorating with gold colloid. In the water solubilization step, some of the sheaves were split in half, as can be seen in Fig. 2F. Aside from this, the morphology of the Fe_2P nanostructures remained the same after functionalization with GABA.

After decorating the precursor with gold colloid, the particles were combined in various amounts (50, 75, 100, 125, and 150 μL) with an aqueous gold plating solution ($HAuCl_4$ and K_2CO_3). Formaldehyde (20 μL) was then introduced to initiate the reduction of gold. Depending on the concentration of precursor particles present, the shell thickness varied, as can be seen in Fig. 3. In the cases where less precursor was added, the gold shell was thicker and excess gold colloid was observed in the TEM images (as seen in Fig. 3A–C).

As the amount of decorated precursor was increased and combined with a constant amount of plating solution, thinner gold shells were formed around the Fe_2P structures. Extinction measurements were taken of the Au–Fe_2P core–shell structures in order to determine their plasmonic properties as a function of shell thickness (Fig. 4). A redshift in the plasmon absorption peak was observed as the shell thickness increased. It is known that the plasmon resonant response of core–shell nanostructures will be dependent upon the core and shell dimensions, as well as the dielectric properties of the core, shell, and embedding medium.[43] In silica-gold core–shell nanostructures, a blueshift is observed as the thickness of the gold shell is increased.[33] Conversely, when iron oxide (Fe_3O_4 or FeO) cores with gold shells were studied, a redshift was observed upon increasing thickness of the gold shell.[16,27] This change in the optical behavior from silica to iron oxide nanoshells has been explained in terms of plasmon hybridization.[27,44,45] The redshift

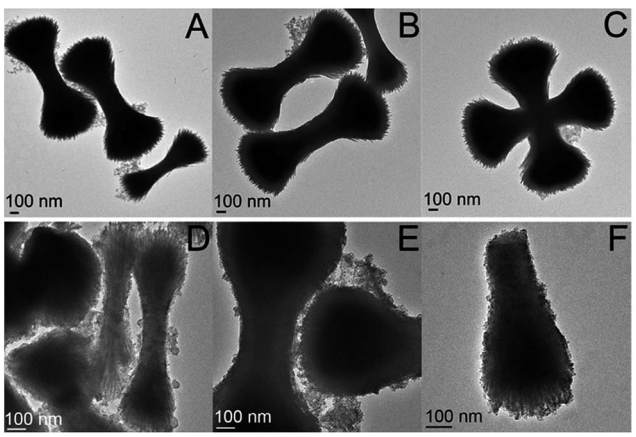

Fig. 2 TEM images of the Fe_2 particles (A–C) as synthesized, dispersed in hexane and (D–F) after being solubilized in water and decorated with Au nanoparticles.

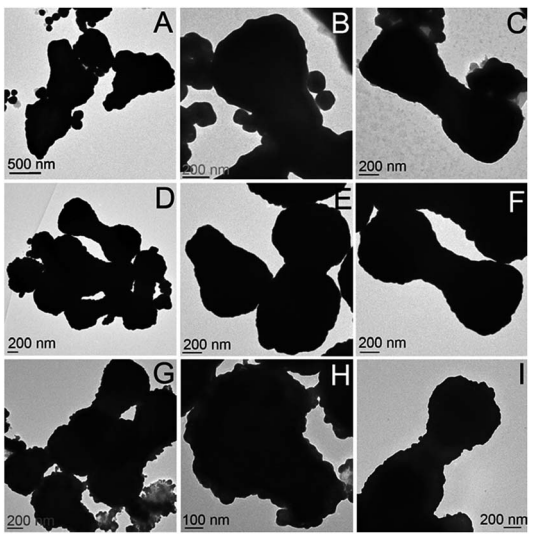

Fig. 3 TEM images of the Fe_2P nanoparticles plated with a gold shell *via* formaldehyde reduction, using (A–C) 50 μL, (D–F) 75 μL, and (G–I) 125 μL of decorated precursor.

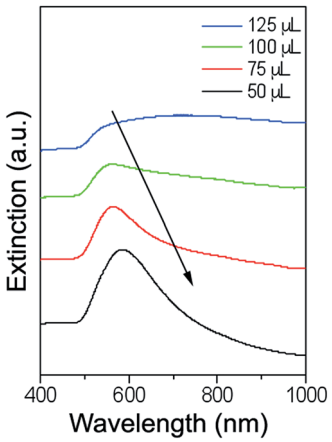

Fig. 4 Solution extinction spectra of the Fe_2P–Au core–shell particles synthesized using formaldehyde reduction (λ_{max} = 584 nm for 50 μL, 565 nm for 75 μL, 559 nm for 100 μL, and 540 nm for 125 μL of decorated precursor). Spectra offset for clarity.

in the plasmon resonance as a function of increasing shell thickness is attributed to the high permittivity of the core iron oxide material (as compared to silica, which has a low permittivity).

Carbon monoxide reduction

Particles synthesized from $H_2Fe_3(CO)_9P^tBu$ in 2 mL TOA and 6 mL OA were used for the experiments using carbon monoxide as the reducing agent. Fig. 5 depicts the Fe_2P nanoparticles before water solubilization with GABA (Fig. 5A and B) and after decorating with gold colloid (Fig. 5C and D).

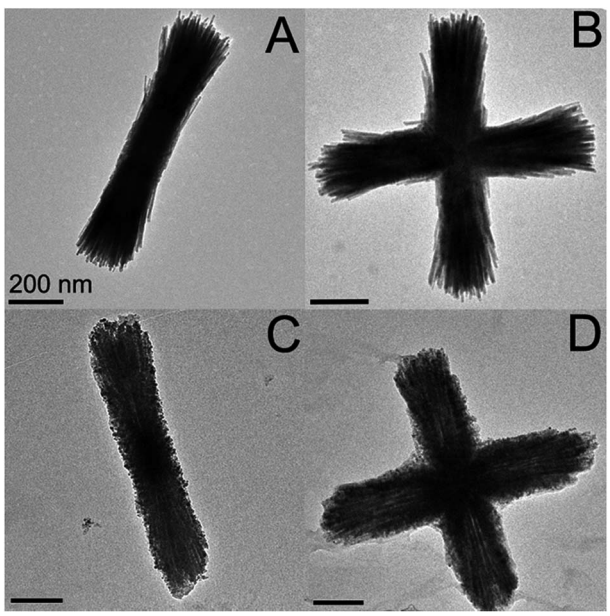

Fig. 5 TEM images of the split Fe_2P rods and crosses. (A and B) Original particles dispersed in hexane and (C and D) particles functionalized with GABA and decorated with small colloidal gold particles. All scale bars are 200 nm.

As was the case with the formaldehyde system, different volumes of decorated precursor were combined with a constant volume of plating solution. These solutions were then bubbled with carbon monoxide for 60 seconds. A representative SEM image for the 50 μL decorated precursor system and TEM images for the 75, 100, and 125 μL decorated precursor systems can be found in the ESI (Fig. S1 and S2).† Extinction measurements were performed on the Fe_2P–Au solutions (Fig. 6). A more thorough presentation of the dimensions of the particles along with aspect ratio and shell thickness information can be found in the Table S1.†

As was seen for the formaldehyde reduced Fe_2P–Au particles, the extinction maximum increased as the shell thickness increased. The absorption for the sample made using 100 μL of decorated precursor redshifted back to higher wavelength, likely due to the fact that some of the Fe_2P structures in this sample were not completely coated with a continuous gold layer (Fig. 7).

Gold nanorods are known to exhibit two surface plasmon modes, longitudinal and transverse, the longitudinal mode occurring at higher wavelengths than the transverse mode. It is expected that the anisotropic Au–Fe_2P structures should exhibit both transverse and longitudinal modes; the values reported here are believed to be of the higher energy transverse modes. Frequency of the longitudinal plasmon mode is known to depend sensitively on variations in aspect ratio[31,40,46] and polarization[31] and can occur into the near infrared (IR).[47,48] Mirkin *et al.* studied the extinction spectra in D_2O of gold rods of various lengths (96, 641, 735, and 1175 nm), all having diameters of ~85 nm.[47] For rods with lengths of 96 nm, the aspect ratio was close to 1, causing the transverse and longitudinal modes to overlap, resulting in one broad peak at ~600 nm. As the aspect ratio was increased, the longitudinal mode shifted to higher wavelengths, with a maximum value of 1410 nm (for the 1175 nm long rods, aspect ratio ~14). There have also been reports of the longitudinal band occurring in the mid IR region for Au, Ni, and Pd nanorods with aspect ratios greater than 25.[49]

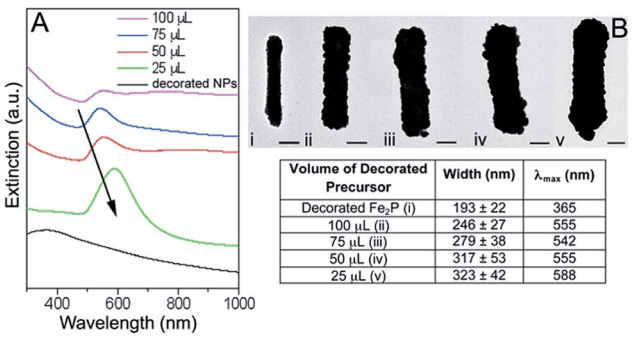

Volume of Decorated Precursor	Width (nm)	λ_{max} (nm)
Decorated Fe_2P (i)	193 ± 22	365
100 μL (ii)	246 ± 27	555
75 μL (iii)	279 ± 38	542
50 μL (iv)	317 ± 53	555
25 μL (v)	323 ± 42	588

Fig. 6 (A) Solution extinction spectra of the carbon monoxide reduction with various decorated precursor volumes (spectra offset for clarity). (B) TEM images of (i) Au-decorated Fe_2P structure and the Fe_2P–Au core–shell structures synthesized by the reduction of Au onto the surface with (ii) 100 μL, (iii) 75 μL, (iv) 50 mL, and (v) 25 μL of decorated precursor. All scale bars are 200 nm.

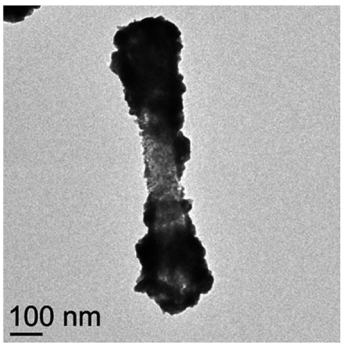

Fig. 7 TEM image of a partially coated Fe_2P nanorod from the sample in which 100 μL of decorated precursor was used.

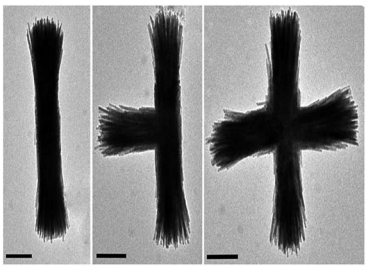

Fig. 8 TEM images of rods, T-shapes, and crosses of unfunctionalized Fe_2P nanoparticles. All scale bars are 200 nm.

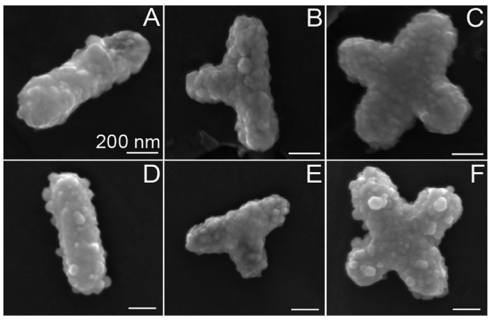

Fig. 9 SEM images of rods, T-shapes, and crosses of the Fe_2P–Au core–shell structures for systems using (A–C) 25 μL and (D–F) 50 mL decorated precursor solutions (100 000× magnification). All scale bars are 200 nm.

Attempts to identify the longitudinal mode for the Au–Fe_2P structures were unsuccessful due to experimental limitations. These measurements will provide more accurate information regarding how the shape of the particle influences the plasmon peaks, as the data presented here were collected as ensemble measurements in water, and there are a variety of shapes and orientations present, as seen in Fig. 8 and 9.

Conclusions

Fe_2P split rods, T-shapes, and crosses were all successfully made water soluble through ligand exchange to replace the hydrophobic oleic acid present on the surface following their synthesis with the smaller GABA ligand. Water solubilization of these structures allowed for them to be coated with a gold shell, the amine group of the GABA serving to bind the colloidal gold particles. The reduction of gold onto the surface of the Fe_2P structures resulted in thinner shell layers without the synthesis of excess gold colloid when the reduction was performed using carbon monoxide as opposed to formaldehyde. Their optical properties were studied, and a redshift in the extinction maximum was seen as the shell thickness increased. This plasmon peak shift, as opposed to the trends seen in silica–Au core–shell structures as shell thickness increases, is attributed to the high permittivity of the Fe_2P core. The same trend has been reported in the coating of iron oxide (Fe_xO–Fe_3O_4) nanoparticles.[27]

Acknowledgements

This material is based upon work supported by the National Science Foundation under Grants No. CHE-0719396 (KHW), CHE-1411495 (KHW), Graduate Research Fellowship under Grant No. 1450681 (DES) and the Robert A. Welch Foundation (KHW: C-0976; NJH: C-1220). This material is based upon work supported by the National Science Foundation.

Notes and references

1 S. L. Brock and K. Senevirathne, *J. Solid State Chem.*, 2008, **181**, 1552–1559.
2 R. Ferrando, J. Jellinek and R. L. Johnston, *Chem. Rev.*, 2008, **108**, 845–910.
3 S. Y. Chou, M. S. Wei, P. R. Krauss and P. B. Fischer, *J. Appl. Phys.*, 1994, **76**, 6673–6675.
4 N. Shukla, C. Liu and A. G. Roy, *Mater. Lett.*, 2006, **60**, 995–998.
5 A.-H. Lu, E. L. Salabas and F. Schüth, *Angew. Chem., Int. Ed. Engl.*, 2007, **46**, 1222–1244.
6 Y.-w. Jun, J.-s. Choi and J. Cheon, *Chem. Commun.*, 2007, 1203–1214, DOI: 10.1039/b614735f.
7 J. Cheon and J.-H. Lee, *Acc. Chem. Res.*, 2008, **41**, 1630–1640.
8 X.-B. Zhang, J.-M. Yan, S. Han, H. Shioyama and Q. Xu, *J. Am. Chem. Soc.*, 2009, **131**, 2778–2779.
9 B. Baruwati, V. Polshettiwar and R. S. Varma, *Tetrahedron Lett.*, 2009, **50**, 1215–1218.
10 W. J. M. Mulder, R. Koole, R. J. Brandwijk, G. Storm, P. T. K. Chin, G. J. Strijkers, C. de Mello Donega, K. Nicolay and A. W. Griffioen, *Nano Lett.*, 2006, **6**, 1–6.
11 M. Kettering, J. Winter, M. Zeisberger, S. Bremer-Streck, H. Oehring, C. Bergemann, C. Alexiou, R. Hergt, K. J. Halbhuber, W. A. Kaiser and I. Hilger, *Nanotechnology*, 2007, **18**, 175101.
12 S. Laurent, D. Forge, M. Port, A. Roch, C. Robic, L. Vander Elst and R. N. Muller, *Chem. Rev.*, 2008, **108**, 2064–2110.
13 Y.-w. Jun, J.-w. Seo and J. Cheon, *Acc. Chem. Res.*, 2008, **41**, 179–189.
14 J. Dobson, *Nat. Nanotechnol.*, 2008, **3**, 139–143.
15 L. Wang, H.-Y. Park, S. I. I. Lim, M. J. Schadt, D. Mott, J. Luo, X. Wang and C.-J. Zhong, *J. Mater. Chem.*, 2008, **18**, 2629–2635.

16 Z. Xu, Y. Hou and S. Sun, *J. Am. Chem. Soc.*, 2007, **129**, 8698–8699.
17 G. Bahmanrokh, M. Hashim, K. A. Matori, M. Navasery, N. Soltani, P. Vaziri, S. Kanagesan, R. Sabbaghizadeh and M. S. Ezzad Shafie, *J. Appl. Phys.*, 2014, **116**, 093907.
18 M. Enders, S. Mukai, T. Uwada and S. Hashimoto, *J. Phys. Chem. C*, 2016, **120**, 6723–6732.
19 D. M. Fouad, W. A. El-Said and M. B. Mohamed, *Spectrochim. Acta, Part A*, 2015, **140**, 392–397.
20 S. Karamipour, M. S. Sadjadi and N. Farhadyar, *Spectrochim. Acta, Part A*, 2015, **148**, 146–155.
21 S. M. Majhi, P. Rai and Y.-T. Yu, *ACS Appl. Mater. Interfaces*, 2015, **7**, 9462–9468.
22 L. Minati, C. L. Cheng, Y. C. Lin, J. Hees, G. Lewes-Malandrakis, C. E. Nebel, F. Benetti, C. Migliaresi and G. Speranza, *Diamond Relat. Mater.*, 2015, **53**, 23–28.
23 T. Mitsudome, M. Yamamoto, Z. Maeno, T. Mizugaki, K. Jitsukawa and K. Kaneda, *J. Am. Chem. Soc.*, 2015, **137**, 13452–13455.
24 L. B. Venarusso, J. Bettini and G. Maia, *ChemElectroChem*, 2016, **3**, 749–756.
25 S.-Y. Ding, J. Yi, J.-F. Li, B. Ren, D.-Y. Wu, R. Panneerselvam and Z.-Q. Tian, *Nat. Rev. Mater.*, 2016, **1**, 16021.
26 Y.-J. Zhang, S.-B. Li, S. Duan, B.-A. Lu, J. Yang, R. Panneerselvam, C.-Y. Li, P.-P. Fang, Z.-Y. Zhou, D. L. Phillips, J.-F. Li and Z.-Q. Tian, *J. Phys. Chem. C*, 2016, **120**, 20684–20691.
27 C. S. Levin, C. Hofmann, T. A. Ali, A. T. Kelly, E. Morosan, P. Nordlander, K. H. Whitmire and N. J. Halas, *ACS Nano*, 2009, **3**, 1379–1388.
28 H. Wang, D. W. Brandl, F. Le, P. Nordlander and N. J. Halas, *Nano Lett.*, 2006, **6**, 827–832.
29 M. Spuch-Calvar, J. Pacifico, J. Pérez-Juste and L. M. Liz-Marzán, *Langmuir*, 2008, **24**, 9675–9681.
30 Yu-Ying, S.-S. Chang, C.-L. Lee and C. R. C. Wang, *J. Phys. Chem. B*, 1997, **101**, 6661–6664.
31 J. Pérez-Juste, I. Pastoriza-Santos, L. M. Liz-Marzán and P. Mulvaney, *Coord. Chem. Rev.*, 2005, **249**, 1870–1901.
32 A. T. Kelly, I. Rusakova, T. Ould-Ely, C. Hofmann, A. Luettge and K. H. Whitmire, *Nano Lett.*, 2007, **7**, 2920–2925.
33 S. J. Oldenburg, R. D. Averitt, S. L. Westcott and N. J. Halas, *Chem. Phys. Lett.*, 1998, **288**, 243–247.
34 D. G. Duff, A. Baiker and P. P. Edwards, *Langmuir*, 1993, **9**, 2301–2309.
35 R. De Palma, S. Peeters, M. J. Van Bael, H. Van den Rul, K. Bonroy, W. Laureyn, J. Mullens, G. Borghs and G. Maes, *Chem. Mater.*, 2007, **19**, 1821–1831.
36 L. Etgar, E. Lifshitz and R. Tannenbaum, *J. Phys. Chem. C*, 2007, **111**, 6238–6244.
37 B. L. Frankamp, N. O. Fischer, R. Hong, S. Srivastava and V. M. Rotello, *Chem. Mater.*, 2006, **18**, 956–959.
38 M. Ghosh, G. Lawes, A. Gayen, G. N. Subbanna, W. M. Reiff, M. A. Subramanian, A. P. Ramirez, J.-P. Zhang and R. Seshadri, *Chem. Mater.*, 2004, **16**, 118–124.
39 K. Somaskandan, T. Veres, M. Niewczas and B. Simard, *New J. Chem.*, 2008, **32**, 201–209.
40 B. E. Brinson, J. B. Lassiter, C. S. Levin, R. Bardhan, N. Mirin and N. J. Halas, *Langmuir*, 2008, **24**, 14166–14171.
41 D. Caruntu, B. L. Cushing, G. Caruntu and C. J. O'Connor, *Chem. Mater.*, 2005, **17**, 3398–3402.
42 D. V. Leff, L. Brandt and J. R. Heath, *Langmuir*, 1996, **12**, 4723–4730.
43 E. Prodan, A. Lee and P. Nordlander, *Chem. Phys. Lett.*, 2002, **360**, 325–332.
44 E. Prodan and P. Nordlander, *J. Chem. Phys.*, 2004, **120**, 5444–5454.
45 E. Prodan, C. Radloff, N. J. Halas and P. Nordlander, *Science*, 2003, **302**, 419–422.
46 M. Grzelczak, A. Sánchez-Iglesias, B. Rodríguez-González, R. Alvarez-Puebla, J. Pérez-Juste and L. M. Liz-Marzán, *Adv. Funct. Mater.*, 2008, **18**, 3780–3786.
47 E. K. Payne, K. L. Shuford, S. Park, G. C. Schatz and C. A. Mirkin, *J. Phys. Chem. B*, 2006, **110**, 2150–2154.
48 N. R. Jana, L. Gearheart and C. J. Murphy, *Adv. Mater.*, 2001, **13**, 1389–1393.
49 G. M. Sando, A. D. Berry and J. C. Owrutsky, *J. Chem. Phys.*, 2007, **127**, 074705.

